J. Hydrol. Hydromech., 61, 2013, 4, 347–351
DOI: 10.2478/johh-2013-0043

The use of sodium polytungstate as an X-ray contrast agent to reduce the beam hardening artifact in hydrological laboratory experiments

Yoshito Nakashima

National Institute of Advanced Industrial Science and Technology (AIST), Geological Survey of Japan, Central 7, Higashi 1-1-1, Tsukuba, Ibaraki 305-8567, Japan.
E-mail: nakashima.yoshito@aist.go.jp

Abstract: Iodine is conventionally used as a contrast agent in hydrological laboratory experiments using polychromatic X-ray computed tomography (CT) to monitor two-phase Darcy flow in porous geological media. Undesirable beam hardening artifacts, however, render the quantitative analysis of the obtained CT images difficult. CT imaging of porous sand/bead packs saturated with iodine and tungsten-bearing aqueous solutions, respectively, was performed using a medical CT scanner. We found that sodium polytungstate ($Na_6H_2W_{12}O_{40}$) significantly reduced the beam hardening compared with potassium iodide (KI). This result is attributable to the location of the K absorption edge of tungsten, which is nearer to the peak of the polychromatic X-ray source spectrum than that of iodine. As sodium polytungstate is chemically stable and less toxic than other heavy element bearing compounds, we recommend it as a promising contrast agent for hydrological CT experiments.

Keywords: Beam hardening artifact; Contrast agent; Darcy flow; Porous media; Sodium polytungstate (SPT); X-ray CT.

INTRODUCTION

Darcy flow experiments using porous geological samples are often performed in laboratory investigation of the hydrology of catchments and vadose zones. X-ray computed tomography (CT) imagery is used to visualize the three-dimensional Darcy flow in complex porous samples (Heindel, 2011; Wildenschild and Sheppard, 2013; Wildenschild et al., 2002; Zhou et al., 2010). The flowing fluid is doped with an X-ray contrast agent to enhance phase differentiation. Iodine is conventionally used as the contrast agent (Heijs et al., 1995; Hirono et al., 2003; Iglauer et al., 2011; Oh et al., 2013; Shi et al., 2011; Watanabe et al., 2013; Wellington and Vinegar, 1987; Werth et al., 2010). However, undesirable beam hardening artifacts (e.g., Ketcham and Carlson, 2001) occur in the obtained CT images when iodine is used with a medical or micro-focus CT scanner having a polychromatic X-ray source. The beam hardening reduces the accuracy of any post-CT outcomes such as image-based porosity calculations (e.g., Uemura et al., 2012). Thus, a better contrast agent is needed.

One way to reduce beam hardening is to use as the contrast agent an element whose K absorption edge is near the peak of the polychromatic X-ray source spectrum (Nakashima and Nakano, 2012). In the present study, a tungsten-bearing electrolyte, namely sodium polytungstate (SPT, $Na_6H_2W_{12}O_{40}$) was examined as a candidate contrast agent for hydrological laboratory CT experiments. Tungsten ($_{74}W$) was chosen because (i) its K absorption edge is located nearer to the peak of the polychromatic X-ray spectrum than that of $_{53}I$ (Fig. 1); (ii) because an SPT solution is aqueous, the bulk density and viscosity of a dilute SPT solution are not quite different from those of pure water that is conventionally used in hydrological flow experiments (see Electronic Supplementary Material for detail); (iii) SPT is chemically stable, commercially available (SOMETU, Berlin, Germany), and significantly less toxic than other heavy element-bearing compounds; and (iv) SPT has been recognized as an X-ray contrast agent in animal science (Stock et al., 2003), although the concentration typically used in that field is too low to determine whether appreciable beam hardening occurs. To demonstrate that beam hardening is significantly reduced by the use of $_{74}W$ instead of $_{53}I$, the following laboratory CT experiments were performed. Homogeneous porous sand and bead pack samples saturated with a heavy element (i.e., tungsten or iodine) bearing aqueous solution were imaged with a medical CT scanner, and the cupping effect (e.g., Remeysen and Swennen, 2006) derived from the beam hardening was quantitatively analyzed using the obtained CT images.

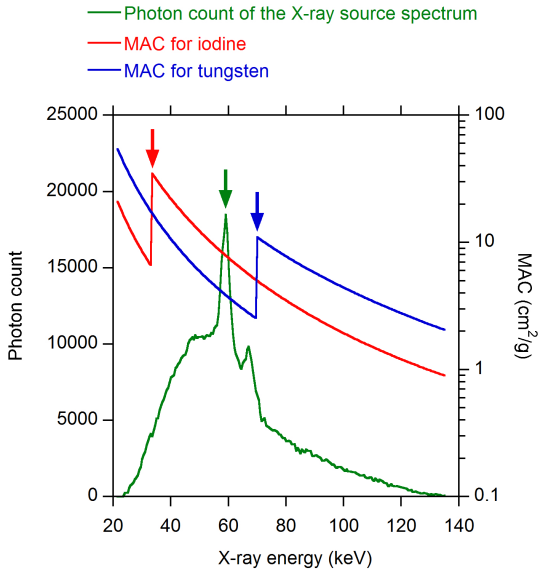

Fig. 1. Photon energy histogram of the primary X-rays emitted from the X-ray tube at an acceleration voltage of 130 kV. The target of the X-ray tube is made of Mo-W alloy. Metal films (Al film of ≈ 1 mm and Cu film of 0.1 mm in thickness) are preinstalled to cut off the undesirable low-energy component (Nakashima, 2003). The mass attenuation coefficient (MAC) spectra for iodine and tungsten, calculated by using the XCOM database (Berger et al., 1998), are superimposed. Arrows show the peak of the X-ray spectrum (59.0 keV) and the K absorption edges of iodine (33.2 keV) and tungsten (69.5 keV).

EXPERIMENTAL

Two granular materials were chosen in the present study to construct porous media packs to be imaged: Toyoura sand and synthetic glass bead. Quartz-rich Toyoura sand from Yamaguchi, Japan, is a standard natural sand sample commonly used in geotechnical research (e.g., Jinguuji et al., 2007; Minagawa et al., 2008). The properties are as follows: grain density, 2.65 g/cm^3; chemical composition, SiO_2, 92.6; Al_2O_3, 3.7; Fe_2O_3, 0.7; CaO, 0.5; MgO, 0.2; loss on ignition, 0.5 wt.% (total, 98.2 wt.%). The sand was packed into a cylindrical tube (inner diameter, 56 mm) made of polypropylene to yield a sand pack porosity of 39 vol.%. Glass beads have been used as a good analogue of well sorted sands in CT experiments (e.g., Clausnitzer and Hopmans, 1999; Wildenschild and Sheppard, 2013), and fine-grained synthetic glass beads (diameter, 0.105–0.125 mm) were employed in the present study (grain density, 2.54 g/cm^3; chemical composition, SiO_2, 72.9; TiO_2, 0.04; Al_2O_3, 1.77; Fe_2O_3, 0.10; CaO, 8.78; MgO, 3.52; Na_2O, 12.18; K_2O, 0.65; P_2O_5, 0.02 wt.% (total, 99.96 wt.%); Nakashima and Watanabe, 2002). The bead grains were packed into the identical cylindrical tube (inner diameter, 56 mm) made of polypropylene to yield a bead pack porosity of 36 vol.%. The porous sand/bead packs were completely saturated with one of two contrast agent solutions as follows: KI = 9.16 and H_2O = 90.84 wt.%; or $Na_6H_2W_{12}O_{40}$ = 8.80 and H_2O = 91.20 wt.%. The experimentally measured bulk density of the KI 9.16 wt.% solution was 1.07 g/cm^3 (Nakashima, 2000), and that of the SPT 8.80 wt.% solution was 1.08 g/cm^3.

The samples were imaged by a third-generation medical CT scanner (W2000, Hitachi Medical Co., Tokyo, Japan) at the Geological Survey of Japan (Nakashima, 2000; Nakashima, 2003; Nakashima and Nakano, 2012; Nakashima et al., 2011) to obtain two-dimensional (2-D) 16-bit TIFF CT images. The imaging conditions were as follows: acceleration voltage, 130 kV; tube current, 100 to 175 mA; slice thickness, 5 mm; field of view of the reconstructed 2-D image, 160^2 mm^2 = 512^2 voxels (three-dimensional voxel dimension, 0.31×0.31×5 mm^3); X-ray exposure time, 4 s; reconstruction filter, Chesler type (standard filter for the human abdomen). No beam hardening correction software was applied to the image reconstruction. The characteristic grain diameter is ≈ 0.3 mm for the Toyoura sand (Minagawa et al., 2008) and ≈ 0. 1 mm for the glass bead used, significantly smaller than the CT slice thickness of 5 mm. Thus, small pore spaces and fine grains were indistinguishable and homogenized in the CT image as a result of the partial-volume effect (Clausnitzer and Hopmans, 1999), and the voxel value distribution within the porous sand/bead pack image should be homogeneous if the beam hardening and filter-derived Gibbs phenomena are both negligible. The following reference samples were also prepared and imaged by the same CT scanner under the same conditions: Toyoura sand and glass bead packed in the identical cylindrical tube saturated with pure water (i.e., without a contrast agent). The effects of the chemistry of the pore fluids and grains on the degree of beam hardening were evaluated by line profile analysis of the voxel values of the CT images. Image processing programs, ImageJ and revised Itrimming.nb (Nakashima and Kamiya, 2007), were used in the post-CT image analysis.

RESULTS

Results of CT imagery and line profile analyses are shown in Figs. 2 and 3 for the Toyoura sand pack and in Figs. 4 and 5 for the glass bead pack. The original CT image (512^2 voxels) was trimmed (240^2 voxels in Figs. 2 and 4). Although a very weak ring artifact (Ketcham and Carlson, 2001) is seen, the CT images are mostly homogeneous due to the partial-volume effect (Clausnitzer and Hopmans, 1999) except for the concentric pattern of the increased voxel value near the sample rim (i.e., cupping effect; Remeysen and Swennen, 2006) caused by the beam hardening.

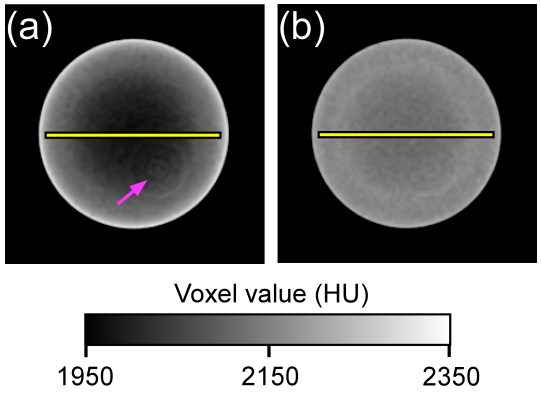

Fig. 2. 2-D CT slices of cylindrical Toyoura sand pack samples (porosity, 39 vol.%; diameter, 56 mm) saturated with a heavy-element-bearing fluid imaged at an acceleration voltage of 130 kV. The sample tube made of polypropylene (thickness 2 mm) is black in the images due to the low density, and indistinguishable from the ambient air. The image dimension is 240^2 voxels = 75^2 mm^2. The image for KI = 9.16 and H_2O = 90.84 wt.% (a) shows marked beam hardening, whereas that for SPT ($Na_6H_2W_{12}O_{40}$) = 8.80 and H_2O = 91.20 wt.% (b) shows very little beam hardening. A very weak ring artifact (arrow) is also seen in (a). Line profiles (shown in Fig. 3) were obtained along the 53-mm-long (i.e., 169-voxel-long) yellow horizontal baselines.

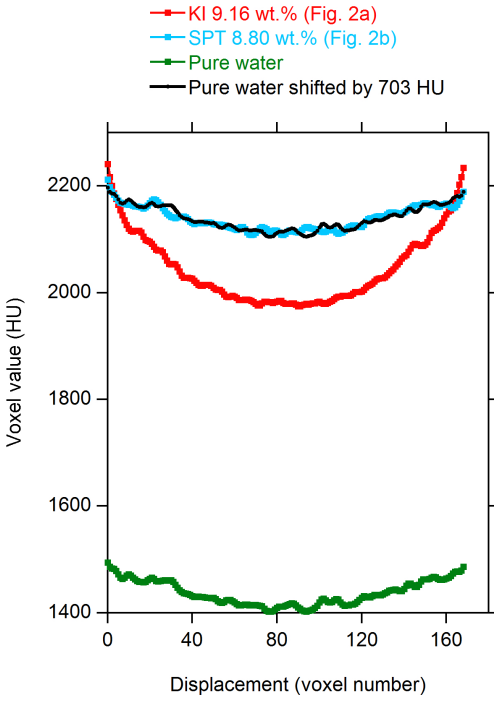

Fig. 3. Line profiles along the yellow baselines of Fig. 2. A line profile for a Toyoura sand pack sample saturated with pure water (i.e., without any contrast agent) is also shown. When the voxel value of the latter is shifted upward by 703 HU, it shows reasonable agreement with the line profile of the SPT 8.80 wt.% solution.

For the line profile analysis shown in Figs. 3 and 5, the one-dimensional distribution of voxel values (in Hounsfield units, HU) along the yellow horizontal baselines (Figs. 2 and 4) crossing the CT images was sampled. Undesirable distortion of the voxel value (e.g., the Gibbs phenomenon) caused by the reconstruction filter occurs around the rim of the sample image (Nakano et al., 2000; Tsuchiyama et al., 2000). Thus, several voxels at each end of the baseline near the rim were discarded, with the result that a 53-mm-long (i.e., 169-voxel-long) baseline was used for a sample with a diameter of 56 mm (i.e., 180 voxels) (Figs. 2 and 4).

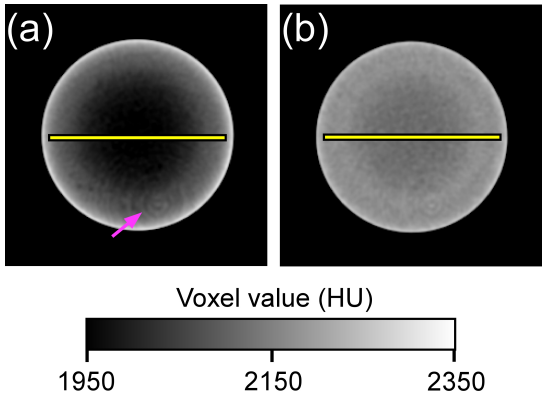

Fig. 4. Same as Fig. 2 but for the glass bead pack samples (porosity, 36 vol.%; diameter, 56 mm). Line profiles (shown in Fig. 5) were obtained along the 53-mm-long (i.e., 169-voxel-long) yellow horizontal baselines.

Two quantities, P_{min} and Δ, were defined and calculated for each line profile to quantify the degree of beam hardening: P_{min} is the minimum line profile value, and Δ is the difference between the maximum and minimum voxel value along the line profile. If the CT image is completely free of beam hardening, then Δ = 0 HU. As for the Toyoura sand pack samples, the (P_{min}, Δ) values in HU were (1975, 266) for the KI 9.16 wt.% solution, (2108, 104) for the SPT 8.80 wt.% solution, and (1402, 92) for the contrast-agent-free water (Fig. 3). The (P_{min}, Δ) values in HU for the glass bead pack samples were (1941, 298) for the KI 9.16 wt.% solution, (2107, 113) for the SPT 8.80 wt.% solution, and (1416, 82) for the contrast-agent-free water (Fig. 5).

DISCUSSION

As noted above, the degree of the beam hardening, Δ, was quite different between iodine and tungsten for both the sand pack and bead pack. With iodine as the contrast agent, the voxel value at both ends of the baseline was almost equal to that for tungsten (Figs. 3 and 5); nevertheless, P_{min} was markedly different between them. This difference demonstrates the advantage of tungsten over iodine via the following simple calculation. When the Toyoura sand packs saturated with the KI solution and pure water are used to calculate the porosity (e.g., Uemura et al., 2011), the difference in P_{min}, 1975–1402 = 573 HU, corresponds to the porosity of 39 vol.%. The porosity estimation error due to the cupping effect (i.e., Δ = 266 HU) is as large as 266×39/573 = 18 vol.%. In contrast, when the sand packs saturated with the SPT solution and pure water are used, the estimation error is reduced to 104 × 39/(2108–1402) = 6 vol.%, demonstrating the advantage of tungsten over iodine. The same calculation could be also applicable to the results for the glass bead (Fig. 5) to obtain the porosity estimation errors of 298 × 36/(1941–1416) = 20 vol.% for KI and 113 × 36/(2107–1416) = 6 vol.% for SPT, which again demonstrates the advantage of tungsten.

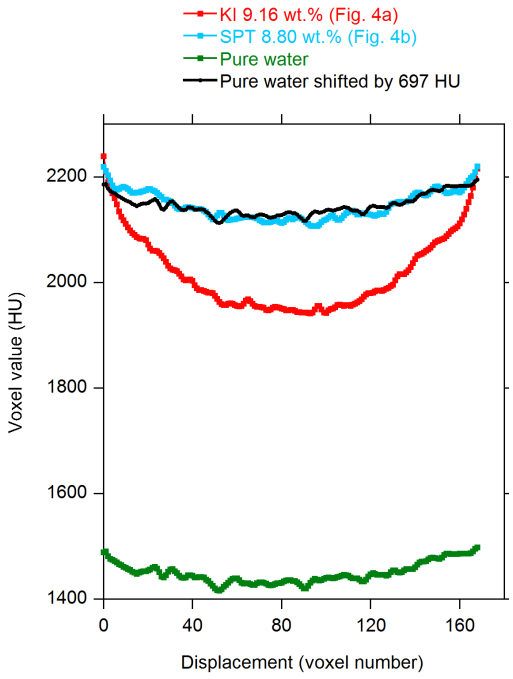

Fig. 5. Same as Fig. 3 but for the glass bead pack samples of Fig. 4. A line profile for a glass bead pack sample saturated with pure water (i.e., without any contrast agent) is also shown. When the line profile for the glass bead pack saturated with contrast-agent-free water is shifted upward by 697 HU, it shows reasonable agreement with the line profile for the SPT 8.80 wt.% solution.

As shown in the above calculation, the (P_{min}, Δ) values of the SiO_2-rich Toyoura sand pack are almost equal to those of the SiO_2-rich bead pack for each pore fluid chemistry (Figs. 3 and 5). Thus, as for the two granular materials examined in the present study, the difference in the grain chemistry yields no marked difference in the beam hardening. This suggests that the advantage of tungsten over iodine also holds for other SiO_2-rich porous geological samples such as sandstones and felsic lavas.

This advantage of tungsten over iodine with respect to the reduction of the cupping effect is a consequence of the physics of beam hardening (Fig. 1): (i) beyond the K absorption edge, X-ray absorption of the heavy element abruptly increases, thus suppressing beam hardening (Cardinal et al., 1993), and (ii) if the K absorption edge of the element used as the contrast agent is located nearer to the peak of the X-ray source spectrum, then the beam hardening is reduced more effectively (Nakashima and Nakano, 2012).

The following example calculation of the degree of fluid replacement in two-phase Darcy flow experiments demonstrates the advantage of using SPT as the contrast agent. The degree of fluid replacement is a critical quantity because it affects the relative permeability of porous media; thus, its accurate measurement by X-ray CT is needed (Shi et al., 2011). Suppose that a homogeneous Toyoura sand pack (diameter, 56 mm; porosity, 39 vol.%) is saturated with contrast-agent-free pure water. Then, a different fluid with a contrast agent is injected into the sand pack, and the replacement of the first fluid with the second in the pore space is monitored over time by X-ray CT. The voxel values of the obtained sand pack images are used to calculate the local degree of fluid replacement, x:

$$x = \frac{V_t - V_{free}}{V_{comp} - V_{free}}, \quad (1)$$

where V_t is the time-dependent local voxel value, V_{free} is the local voxel value before the injection of the contrast agent-bearing fluid, and V_{comp} is that after the fluid replacement of all pores has been completed (Uemura et al., 2011). For the two tested contrast agents, KI 9.16 wt.% (Fig. 2a) and SPT 8.80 wt.% (Fig. 2b), the denominator on the right-hand side of Eq. (1) at both ends of the baseline is about 700 HU for both contrast agent solutions (Fig. 3). Beam hardening causes the voxel value in the numerator of the right-hand side of Eq. (1), to fluctuate, producing undesirable systematic noise and resulting in an estimation error of x. The use of KI 9.16 wt.% solution could increase an estimation error of x by (266–104)/700 ≈ 23 % compared with the use of the SPT 8.80 wt.% solution (the numbers, 266 and 104, are the Δ values for KI and SPT, respectively in Fig. 3). An increase in the error as large as 23 % can critically affect the calculation of the relative permeability diagram (Shi et al., 2011). In contrast, if the line profile for the sand pack saturated with pure water is shifted upward by 703 HU, it almost overlaps the line profile for the SPT 8.80 wt.% solution (Fig. 3). This result suggests that the value of Δ is constant at ≈100 HU and independent of the concentration of the SPT solution for any SPT concentration between 0 and 8.80 wt.%. Thus, the estimation error due to the additional beam hardening by the use of SPT is almost negligible during the fluid replacement in the Toyoura sand pack. The same discussion using Eq. (1) was also applied to the results for the glass bead pack (Fig. 5). It showed that the use of KI 9.16 wt.% solution could increase an estimation error of x by (298–113)/700 ≈ 26 % compared with the use of the SPT 8.80 wt.% solution. The agreement of the line profile for pure water shifted upward by 697 HU and that for the SPT 8.80 wt.% solution was also observed. These examples demonstrate the advantage of SPT over KI.

The advantage of tungsten over iodine is a consequence of the physics of beam hardening, and should be independent of the detail of the medical CT scanner. To confirm the independence, the same Toyoura sand pack samples were imaged using a different third-generation medical CT scanner (PRATICO-FR, Hitachi Medical Co., Tokyo, Japan) at the same acceralation voltage, reconstruction filter, voxel dimensions, exposure time, and field of view (Nakashima, unpublished data). The obtained (P_{min}, Δ) values in HU were (1785, 209) for the KI-bearing sample of Fig. 2a, and (1889, 54) for the SPT-bearing sample of Fig. 2b. These values are slightly different from those in Fig. 3 probably due to the slight difference in the X-ray source spectrum and/or calibration detail of the CT apparatus. However, because the Δ value for the SPT-bearing sample (54 HU) is significantly smaller than that for the KI-bearing sample (209 HU), the results by the PRATICO-FR scanner confirm the advantage of tungsten over iodine with respect to beam hardening reduction.

The present study reports the successful reduction of the cupping effect (non-uniform voxel value distribution inside *homogeneous* porous media) by the use of SPT. Another beam-hardening-derived artifact different from the cupping artifact can occur for the hydrological CT of the preferential flow in macroscopic pipes/fractures inside *heterogeneous* porous media; it is a dark streak which arises between two pipes/fractures having bright voxel values (Remeysen and Swennen, 2006). The dark streak artifact reduces the accuracy of post-CT outcomes such as image-based porosity calculations. Remeysen and Swennen (2006) reported that the reduction of the cupping artifact also yields the reduction of the dark streaks. Thus, the use of SPT probably contributes to the reduction of the dark streak artifact critical for the hydrological CT experiments of the preferential flow in macroscopic pipes/fractures.

CONCLUSIONS

Laboratory X-ray CT experiments were performed to compare the performance of KI and $Na_6H_2W_{12}O_{40}$ as the contrast agent in a porous sand/bead pack with respect to beam hardening reduction. KI, the most commonly used contrast agent in hydrology, is not recommended because its use resulted in a marked beam hardening artifact. In contrast, the use of a tungsten compound, $Na_6H_2W_{12}O_{40}$, significantly reduced the beam hardening compared with the KI result. Therefore, $Na_6H_2W_{12}O_{40}$ is recommended as a better contrast agent in hydrological laboratory experiments.

Acknowledgements. Comments by anonymous reviewers were helpful. The public domain program, ImageJ, developed by the National Institutes of Health and available at http://imagej.nih.gov/ij/ was used for image processing (e.g., line profile analysis) of the CT images. The CT experiment using the PRATICO-FR scanner was performed under the cooperative research program of Center for Advanced Marine Core Research (CMCR), Kochi University (13B034) with the support of JAMSTEC.

REFERENCES

Berger, M.J., Hubbell, J.H., Seltzer, S.M., Chang, J., Coursey, J.S., Sukumar, R., Zucker, D.S., Olsen, K., 1998. XCOM: Photon Cross Sections Database. National Institute of Standards and Technology. http://www.nist.gov/pml/data/xcom/index.cfm/

Cardinal, H.N., Holdsworth, D.W., Drangova, M., Hobbs, B.B., Fenster, A., 1993. Experimental and theoretical x-ray imaging performance comparison of iodine and lanthanide contrast agents. Med. Phys., 20, 15–31.

Clausnitzer, V. Hopmans, J.W., 1999. Determination of phase-volume fractions from tomographic measurements in two-phase systems. Adv. Water Resour., 22, 577–584.

Heijs, A.W., De Lange, J., Schoute, J.F.Th., Bouma, J., 1995. Computed tomography as a tool for non-destructive analysis of flow patterns in macroporous clay soils. Geoderma, 64, 183–196.

Heindel, T.J., 2011. A review of X-ray flow visualization with applications to multiphase flows. J. Fluids Eng., 133, article number 074001.

Hirono, T., Takahashi, M., Nakashima, S., 2003. In situ visualization of fluid flow image within deformed rock by X-ray CT. Eng. Geol., 70, 37–46.

Iglauer, S., Paluszny, A., Pentland, C.H., Blunt, M.J., 2011. Residual CO_2 imaged with X-ray micro-tomography. Geophys. Res. Lett., 38, L21403.

Jinguuji, M., Toprak, S., Kunimatsu, S., 2007. Visualization technique for liquefaction process in chamber experiments by using electrical resistivity monitoring. Soil Dyn. Earthq. Eng., 27, 191–199.

Ketcham, R.A., Carlson, W.D., 2001. Acquisition, optimization and interpretation of X-ray computed tomographic imagery: applications to the geosciences. Comp. Geosci., 27, 381–400.

Minagawa, H., Nishikawa, Y., Ikeda, I., Miyazaki, K., Takahara, N., Sakamoto, Y., Komai, T., Narita, H., 2008. Characterization of sand sediment by pore size distribution and permeability using proton nuclear magnetic resonance measurement. J. Geophys. Res., 113, article number B07210.

Nakano, T., Nakashima, Y., Nakamura, K., Ikeda, S., 2000. Observation and analysis of internal structure of rock using X-ray CT. J. Geol. Soc. Jpn., 106, 363–378.

Nakashima, Y., 2000. The use of X-ray CT to measure diffusion coefficients of heavy ions in water-saturated porous media. Eng. Geol., 56, 11–17.

Nakashima, Y., 2003. Diffusivity measurement of heavy ions in Wyoming montmorillonite gels by X-ray computed tomography. J. Contam. Hydrol., 61, 147–156.

Nakashima, Y., Kamiya, S., 2007. Mathematica programs for the analysis of three-dimensional pore connectivity and anisotropic tortuosity of porous rocks using X-ray computed tomography image data. J. Nucl. Sci. Technol., 44, 1233–1247.

Nakashima, Y., Nakano. T., 2012. Nondestructive quantitative analysis of a heavy element in solution or suspension by single-shot computed tomography with a polychromatic X-ray source. Anal. Sci., 28, 1133–1138.

Nakashima Y., Watanabe, Y., 2002. Estimate of transport properties of porous media by micro-focus x-ray computed tomography and random walk simulation. Water Resour. Res., 38, article number 1272.

Nakashima, Y., Mitsuhata, Y., Nishiwaki, J., Kawabe, Y., Utsuzawa, S., Jinguuji, M., 2011. Non-destructive analysis of oil-contaminated soil core samples by X-ray computed tomography and low-field nuclear magnetic resonance relaxometry: a case study. Water Air Soil Pollut., 214, 681–698.

Oh, J., Kim, K.Y., Han, W.S., Kim, T., Kim, J.C., Park, E., 2013. Experimental and numerical study on supercritical CO_2/brine transport in a fractured rock: Implications of mass transfer, capillary pressure and storage capacity. Adv. Water Resour., (in press).

Remeysen, K., Swennen, R., 2006. Beam hardening artifact reduction in microfocus computed tomography for improved quantitative coal characterization. Int. J. Coal Geol., 67, 101–111.

Shi, J.Q., Xue, Z., Durucan, S., 2011. Supercritical CO_2 core flooding and imbibition in Tako sandstone–influence of subcore scale heterogeneity. Int. J. Greenh. Gas Control, 5, 75–87.

Stock, S.R., Nagaraja, S., Barss, J., Dahl, T., Veis, A., 2003. X-ray microCT study of pyramids of the sea urchin Lytechinus variegatus. J. Struct. Biol., 141, 9–21.

Tsuchiyama, A., Hanamoto, T., Nakashima, Y., Nakano, T., 2000. Quantitative evaluation of attenuation contrast of minerals by using a medical X-ray CT scanner. J. Miner. Petrol. Sci., 95, 125–137.

Uemura, S., Fukabori, D., Tsushima, S., Hirai, S., 2012. Visualization and analysis of CO_2 permeation process in a porous media by microfocus X-ray computed tomography. Trans. Jpn. Soc. Mech. Eng. Ser B, 78, 74–82.

Uemura, S., Kataoka, R., Fukabori, D., Tsushima, S., Hirai, S., 2011. Experiment on liquid and supercritical CO_2 distribution using micro-focus X-ray CT for estimation of geological storage. Energy Procedia, 4, 5102–5107.

Watanabe, N., Ishibashi, T., Tsuchiya, N., Ohsaki, Y., Tamagawa, T., Tsuchiya, Y., Okabe, H., Ito, H., 2013. Geologic core holder with a CFR PEEK body for the X-ray CT-based numerical analysis of fracture flow under confining pressure. Rock Mech. Rock Eng., 46, 413–418.

Wellington, S.L. Vinegar, H.J., 1987. X-ray computerized tomography. J. Petrol. Technol., 39, 885–898.

Werth, C.J., Zhang, C., Brusseau, M.L., Oostrom, M., Baumann, T., 2010. A review of non-invasive imaging methods and applications in contaminant hydrogeology research. J. Contam. Hydrol., 113, 1–24.

Wildenschild, D., Sheppard, A.P., 2013. X-ray imaging and analysis techniques for quantifying pore-scale structure and processes in subsurface porous medium systems. Adv. Water Resour., 51, 217–246.

Wildenschild, D., Vaz, C.M.P., Rivers, M.L., Rikard, D., Christensen, B.S.B., 2002. Using X-ray computed tomography in hydrology: systems, resolutions, and limitations. J. Hydrol., 267, 285–297.

Zhou, N., Matsumoto, T., Hosokawa, T., Suekane, T., 2010. Pore-Scale visualization of gas trapping in porous media by X-ray CT scanning. Flow Meas. Instrum., 21, 262–267.

Received 2 May 2013
Accepted 17 July 2013

Note: Supplementary material can be found in the web version of this article.

SUPPLEMENTARY MATERIAL

Additional information about the properties of the SPT solution

SPT has been used in geosciences as a heavy liquid for the separation of minerals (e.g., Gregory and Johnston, 1987; Munsterman and Kerstholt, 1996; Conceição et al., 2008). Thus, some data on the properties of the aqueous solutions of SPT are available. For example, the bulk density, viscosity, and electric conductivity are reported by Torresan (1987). The bulk density, viscosity, and pH are noted in Skipp and Brownfield (1993). According to the literature, as for the low-concentration SPT solution used in the present study (i.e., 8.80 wt.%), the bulk density and viscosity are about 1.1 g/cm^3 and 1 mPa·s, respectively. Because these values are almost equal to those for pure water (i.e., 1.0 g/cm^3 and 1 mPa·s, respectively), the dilute SPT solution can be a reasonable substitute for pure water that is conventionally used in hydrological flow experiments.

REFERENCES

Conceição, P.C., Boeni, M., Dieckow, J., Bayer, C., Mielniczuk, J., 2008. Fracionamento densimétrico com politungstato de sódio no estudo da proteção física da matéria orgânica em solos. R. Bras. Ci. Solo, 32, 541–549.

Gregory, M.R., Johnston, K.A., 1987. A nontoxic substitute for hazardous heavy liquid – aqueous sodium polytungstate ($3Na_2WO_4$. $9WO_3$. H_2O) solution. N. Z. J. Geol. Geophys., 30, 317–320.

Munsterman, D., Kerstholt, S., 1996. Sodium polytungstate, a new non-toxic alternative to bromoform in heavy liquid separation. Rev. Palaeobot. Palynology, 91, 417–422.

Skipp, G.L., Brownfield, I., 1993. Improved density gradient separation techniques using sodium polytungstate and a comparison to the use of other heavy liquids. US Geological Survey. Open-File Report, 92–386.

Torresan, M., 1987. The use of sodium polytungstate in heavy mineral separations. US Geological Survey. Open-File Report, 87–590.